

# Dynamic Pedestrian Traffic Assignment with Link Transmission Model for Bidirectional Sidewalk Networks

Tanapon Lilasathapornkit<sup>a</sup>, Meead Saberi<sup>a,\*</sup>

<sup>a</sup>Research Centre for Integrated Transport Innovation (rCITI), School of Civil and Environmental Engineering, University of New South Wales, Sydney, NSW, Australia

## ARTICLE INFO

### Keywords:

Bidirectional pedestrian flow  
Dynamic network loading  
Link transmission model  
Dynamic user equilibrium

## ABSTRACT

Planning assessment of the urban walking infrastructure requires appropriate methodologies that can capture the time-dependent and unique microscopic characteristics of bidirectional pedestrian flow. In this paper, we develop a simulation-based dynamic pedestrian traffic assignment (DPTA) model specifically formulated for walking networks (e.g. sidewalks) with bidirectional links. The model consists of a dynamic user equilibrium (DUE) based route choice and a link transmission model (LTM) for network loading. The formulated DUE adopts a pedestrian volume delay function (pVDF) taking into account the properties of bidirectional pedestrian streams such as self-organization. The adopted LTM uses a three-dimensional triangular bidirectional fundamental diagram as well as a generalized first-order node model. The applicability and validity of the model is demonstrated in hypothetical small networks as well as a real-world large-scale network of sidewalks in Sydney. The model successfully replicates formation and propagation of shockwaves in walking corridors and networks due to bidirectional effects.

## 1. Introduction

Potential health and societal benefits of active transportation are becoming more acknowledged. Many cities around the world are increasing their investment in walking infrastructure. However, overcrowded footpaths in some cities during peak hours create potential safety risks and increase delays for pedestrians. Investment in walking infrastructure is often made on an adhoc manner rarely supported by strategic large-scale pedestrian network models similar to what is commonly used for analysis of vehicular traffic systems.

Urban footpaths or sidewalks can be viewed as a network of bidirectional pedestrian links. Several studies in the past have already investigated the bidirectional crowd dynamics using the fundamental relationship between flow and density (Seyfried et al. 2005, Zhang et al. 2012, Hänseler et al. 2014, Cao et al. 2017, Hänseler et al. 2017, Saberi and Mahmassani 2014, Saberi, Aghabayk, and Sobhani 2015). Despite its significance and practical relevance, very little effort has been put into understanding and modeling the network-wide impact of pedestrian traffic in the urban context for planning applications. This study aims to develop a simulation-based dynamic pedestrian traffic assignment (DPTA) framework to model large-scale footpath or sidewalk networks.

Research on pedestrian flow modeling and dynamics has grown in several directions in the past few decades including development of novel approaches in microscopic modeling (Løvås 1994, Helbing and Molnar 1995, ?, Moussaïd et al. 2010, Huang et al. 2017, Tao and Dong 2017, Shahhoseini, Sarvi, and Saberi 2018), mesoscopic modeling (Xiong et al. 2010, Cristiani, Piccoli, and Tosin 2011, Tordeux et al. 2018), and macroscopic simulation (Hughes 2002, Colombo, Garavello, and Lécureux-Mercier 2011, Schwandt, Huth, and Bärwolff 2013, Hoogendoorn et al. 2015, Hänseler et al. 2017, Hoogendoorn et al. 2018, Taherifar et al. 2019, Aghamohammadi and Laval 2020, Moustaid and Flötteröd 2021, Molyneaux, Scarinci, and Bierlaire 2021). For a detailed review of the literature on pedestrian crowd data collection and empirical insights, see (Haghani and Sarvi 2018, Haghani 2020a,b).

Simulation-based dynamic traffic assignment (DTA) models are used as tools to provide estimates of traffic conditions for transportation operations applications and are increasingly applied in strategic transportation planning to support decision making of infrastructure investments. Two main reasons that have led to increasing popularity of DTA developments in practice in the past few decades are as follows. Firstly, the static traffic assignment model does not sufficiently capture congestion dynamics in the network including oversaturation, formation of physical queues, spillbacks, and shockwaves (Raadsen, Bliemer, and Bell 2016, Bliemer and Raadsen 2019). In a previous study by Lilasathapornkit et al. (2020), a static traffic assignment modeling framework with bidirectional link performance functions is already proposed. Secondly, implementation of a sub-daily traffic model requires anticipation of spatial

and temporal changes in traffic conditions that could result in re-routing or traffic accumulation in certain areas of the network (Melson et al. 2018). Simulation-based DTA models capture the essential dynamic properties of traffic flow including planned interruptions such as signal control (Zhu and Ukkusuri 2015) or unplanned disruptions such as capacity reduction due to incidents (He and Liu 2012, Nogal et al. 2016). A large body of research already exists that looks into increasing the efficiency and accuracy of traffic simulation models in large-scale networks while retaining the most essential characteristics of traffic flow (Saeedmanesh and Geroliminis 2017, Yildirimoglu, Sirmatel, and Geroliminis 2018, Batista and Leclercq 2019, Han, Eve, and Friesz 2019). Aghamohammadi and Laval (2020) provides a comprehensive literature review on DTA modeling for both pedestrians and vehicles. In this study, we build upon the rich literature of simulation-based DTA and develop the first dynamic sidewalk network model that takes into account the microscopic behaviour of bidirectional pedestrian traffic flow such as self-organization.

Network traffic user equilibrium (UE) problem can be formulated as Variational Inequality (VI) in the context of static traffic assignment (Dafermos 1980) and dynamic networks (Friesz et al. 1993, Ran, Hall, and Boyce 1996, Bliemer 2001, Friesz et al. 2011, Gentile 2016). However, the main difficulty with the analytical DTA approach is adding realistic traffic dynamics to an already sophisticated formulation. Reproducing the formation, propagation, and dissipation of physical queues across multiple links are not a trivial task. The seminal LWR model uses the kinematic wave theory to address this limitation (Lighthill and Whitham 1955, Richards 1956). To solve the LWR problem, Daganzo (1994, 1995a) proposed the cell transmission model (CTM) that discretizes time and space and provides approximate solutions. A few years later Yperman, Logghe, and Immers (2005) proposed the link transmission model (LTM) that discretizes time and link boundary conditions based on Newell's simplified formulation of kinematic wave theory (Newell 1993). LTM often yields a more accurate solution than CTM with the same time-step size and less computational cost (Jin 2015). During the past decade, LTM has become an increasingly popular model for dynamic network loading (DNL) (Gentile et al. 2010, Himpe, Corthout, and Tampère 2016, Raadsen, Bliemer, and Bell 2016, Chakraborty et al. 2018, Bliemer and Raadsen 2019, Raadsen and Bliemer 2019). In this study, we adopt a similar LTM approach and integrate it into a simulation-based DTA to model footpath networks with bidirectional links.

The main contributions of this study are as follows: (i) We formulate a DUE problem that adopts a travel cost function appropriate for bidirectional pedestrian streams calibrated with data from controlled experiments; (ii) We propose and calibrate new bidirectional three-dimensional pedestrian fundamental diagrams for traffic assignment applications; (iii) We also propose a new node model to accommodate for the bidirectional pedestrian flows within the LTM; (iv) We demonstrate the applicability and validity of the model in both small and large-scale pedestrian networks. The paper provides a balance between mathematical rigor on one hand and realism on the other. The proposed pedestrian simulation-based DTA framework adopts the classical DUE with flow-based cost functions for the route choice model and the LTM for DNL. To the best knowledge of the authors, this is the first study in the literature that presents a large-scale LTM-based DPTA model for bidirectional sidewalk networks.

The remainder of the paper is organized as follows. A review of the literature on route choice models and DNL is provided in Section 2.1 and Section 2.2. Section 3 presents the numerical results including a small grid network, a long corridor and a large-scale sidewalk network of Sydney. Section 4 summarizes the contributions and suggests future research directions.

## 2. Methodology

A DTA model consists of two general components: the route choice model and the DNL. In the following, we describe the methodological details of both components in our developed approach as illustrated in Figure 1.

### 2.1. Route choice model

Link travel times vary over time depending on the prevailing traffic conditions. Link travel times can be estimated based on link inflow (Jang, Ran, and Choi 2005, Bliemer and Bovy 2003, Gentile 2016), occupancy (Lo and Szeto 2002, Daganzo 1995b), or horizontal difference between cumulative counts (Tong and Wong 2000, Nie and Zhang 2010, Friesz et al. 2013). In this study, we will use an inflow based link travel time function extended from our previous work on pedestrian volume delay functions (Lilasathapornkit et al. 2020).

In the early DTA models, equilibrium conditions were often based on instantaneous path cost (Friesz et al. 1993) as in static traffic assignment models. However, more recent implementations of DTA often include experienced path cost instead (Chiu et al. 2011). In this study, travellers are assumed to have a perfect knowledge of the network including current travel costs (instantaneous path cost), but do not have the knowledge of their actual travel cost (experienced

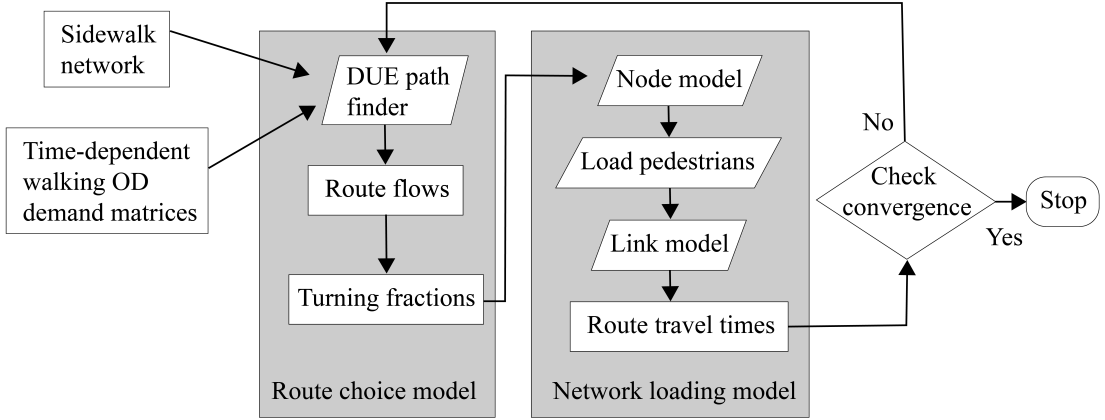


**Figure 1:** An overview of the proposed DPTA model.

path cost). Assignment of traffic based on instantaneous route travel times is not necessarily incorrect, but it is under assumption that travellers decide to take the shortest route using pre-trip travel information (Ran, Boyce, and LeBlanc 1993, Chiu et al. 2011, Chen and Rakha 2014, Yildirimoglu and Geroliminis 2013).

A DUE algorithm iteratively updates route choices over the entire network until all users going from origin  $r$  to destination  $s$  at time  $t$  share the same minimal expected travel time. Solving DUE with continuous time variable may not be practical in large-scale networks, so discrete time formulation is often utilized (Chen and Hsueh 1998, Bliemer and Bovy 2003). Yperman, Logghe, and Immers (2005) introduced the first LTM based on a simplified kinematic wave theory with a discrete time. Several studies in the past aimed to reduce LTM computation time by proposing efficient iterative algorithms (Himpe, Corthout, and Tampère 2016), event-based algorithms (Raadsen, Bliemer, and Bell 2016), and continuous algorithms (Han, Piccoli, and Szeto 2016, Gentile 2016, Raadsen and Bliemer 2019). In this study, we use a discrete-time approach.

Building upon the Wardrop's first principle (Wardrop 1952), we use the DUE condition in which travelers route choice is based on the minimum instantaneous route costs. However, the DNL, as will be described later in the paper, estimates link and route travel times based on a triangular fundamental diagram that estimates the actual (experienced) route travel costs. The two route travel time estimates are expected to be highly correlated as shown later in the numerical experiments section of the paper.

### 2.1.1. Dynamic User Equilibrium.

Let  $G = (N, A)$  be the directed graph consisting of nodes  $N$  and links  $A$ . Let  $\mathbf{c}$  be the vector of link travel time functions,  $\mathbf{u}$  be the vector of link flows,  $\bar{\mathbf{u}}$  be the vector of optimized link flow,  $S$  be a set of feasible link flow patterns,  $K$  be a set of discrete departing time instants,  $T$  be a set of discrete time instants,  $u_a$  be the pedestrian flow on link  $a \in A$ ,  $N$  be a set of nodes,  $\Pi_{rs}$  denotes the set of paths connecting OD pair  $(r, s) \in W$ . Let  $c_{a,t}(u_{a,t})$  be the walking travel time on link  $a \in A$  as a function of the link flow  $u_{a,t}$  at time instant  $t$ ,  $c_{p,k}^{rs}$  be the path travel time on path  $p$  at the departure time  $k \in K$ ,  $\delta_{a,p,k,t}^{rs}$  be the link-path incidence matrix at time  $t$ ,  $f_k^{rs}$  be the flow on path  $p$  at the departure time  $k$  connecting an OD pair  $(r, s) \in W$ , and  $q_k^{rs}$  be the travel demand between OD pair  $(r, s)$  at the departure time  $k$ . Wardrop (1952)'s first principle states that at UE, no traveler has any incentive to unilaterally change its route. Therefore, the traffic assignment problem (TAP) can be formulated as a variational inequality problem VI( $\mathbf{c}, S$ ) that finds the optimal link flows  $\bar{\mathbf{u}}$  as expressed in Equation (1).

$$\begin{aligned}
 & \mathbf{c}(\bar{\mathbf{u}})(\mathbf{u} - \bar{\mathbf{u}}) \geq 0 & \forall \mathbf{u}, \bar{\mathbf{u}} \in S & (1a) \\
 \text{subject to: } & u_{a,t} = \sum_{r \in N} \sum_{s \in N} \sum_{p \in \Pi_{rs}} \sum_{k \in K} \delta_{a,p,k,t}^{rs} f_{p,k}^{rs} & \forall a \in A, \forall t \in T & (1b) \\
 & \sum_{p \in \Pi_{rs}} f_{p,k}^{rs} = q_k^{rs} & \forall (r, s) \in W, \forall k \in K & (1c)
 \end{aligned}$$

$$f_{p,k}^{rs} \geq 0 \quad \forall (r, s) \in W, \forall p \in \Pi_{rs}, \forall k \in K \quad (1d)$$

$$c_{p,k}^{rs} = \sum_{a \in A} \sum_{t \in T} c_{a,t} \delta_{a,p,k,t}^{rs} \quad \forall p \in \Pi_{rs}, \forall k \in K \quad (1e)$$

### 2.1.2. Link travel time function

Here, we use our previously developed pedestrian volume delay function (pVDF) in Lilasathapornkit et al. (2020). Consider a pair of link  $a, a' \in A$  that belongs to the same bidirectional stream. Let  $\tau_a$  denotes the free flow travel time of link  $a$ ,  $C_a$  denotes the capacity of link  $a$ , and  $\alpha$  and  $\beta$  be model parameters. We denote

$$c_{a,t}(u_{a,t}, u_{a',t}) = \tau_a \left( 1 + \alpha \left( \frac{u_{a,t} + u_{a',t}}{C_a} \right)^\beta \right) \quad \forall a, a' \in A, \forall t \in T \quad (2)$$

the deterministic symmetric pVDF of link  $a \in A$  for time  $t \in T$ . Equation (2) represents a pVDF with symmetric link interactions that is extended from the well-known BPR function with  $\alpha$  representing the ratio of travel time per unit distance at practical capacity to that at free flow while  $\beta$  determines how fast the average travel time increases from free-flow to congested conditions. Links from both directions of the same bidirectional stream have identical travel times. Equation (2) also implies that flows from either directions have equivalent impact on travel time of both directions.

We also consider an asymmetric pVDF as follows where  $\alpha, \beta, \mu, \eta_r, \lambda_r, \eta_c$ , and  $\lambda_c$  are the model parameters. We denote

$$c_{a,t}(u_{a,t}, u_{a',t}) = \tau_a \left( 1 + \alpha \left( \frac{u_{a,t} + u_{a',t}}{C_a} \right)^\beta \right) + \tau_a \mu e^{\eta_r \left( \frac{u_{a,t}}{C_a} - \lambda_r \right)^2 + \eta_c \left( \frac{u_{a',t}}{C_a} - \lambda_c \right)^2} \quad \forall a, a' \in A, \forall t \in T \quad (3)$$

the deterministic asymmetric pVDF of link  $a \in A$  for time  $t \in T$ .

The first term in Equation (3) is the same as that in Equation (2). The second term, referred to as the bidirectional term, captures the bidirectional pedestrian flow in which as pedestrian flows get closer to a certain value ( $\eta_r$  for the reference direction and  $\eta_c$  for the counter direction), the travel time substantially increases. The bidirectional term becomes negligible when flows are further away from these values ( $\eta_r$  and  $\eta_c$ ). The term consists of five parameters.  $\mu$  determines the magnitude of the bidirectional impact for the balanced flows.  $\eta_r$  and  $\eta_c$  determine the range of flows that exhibit bidirectional impact by regulating the width of a bell-shaped curve base.  $\lambda_r$  and  $\lambda_c$  determine the flow ratios that have the highest congestion level in the stream. In this study, we use the proposed link travel time functions in Lilasathapornkit et al. (2020) as the cost functions in the route choice model. The estimated travel time is treated as a pre-trip expected travel time used to find the DUE.

### 2.1.3. Turning fraction

The distribution of flows from incoming links toward outgoing links is obtained from the total turning fraction. Let  $\phi_{ij}^n$  be the turning fraction from incoming link  $i$  toward outgoing link  $j$  through node  $n \in N$ . We denote

$$0 \leq \phi_{ij}^n \leq 1, \quad \forall i, j \in A, \forall n \in N \quad (4a)$$

$$\sum_j \phi_{ij}^n = 1, \quad \forall i \in A, \forall n \in N \quad (4b)$$

We derive the turning fractions from the output of the DUE by converting all route flows toward the same destination into a set of turning fractions at each time instant. For example if we have 3 origins and 2 destinations, 2 sets of turning fractions will be determined.

## 2.2. Dynamic network loading

A first order DNL model consists of a link model and a node model often based on kinematic wave theory (Lighthill and Whitham 1955, Richards 1956) in which vehicles are represented as flows that propagate in the network. The link model defines flow propagation within each link boundary while the node model regulates how upstream links

distribute flows toward downstream links at each node. Here, we propose a pedestrian triangular fundamental diagram that captures bidirectional interactions in walking streams. The DNL model loads users into associated routes through the network from the origin nodes towards the destination nodes. We use LTM as our DNL model due to its calculation efficiency (Yperman, Logghe, and Immers 2005). LTM consists of the flow model which follows a modified kinematic wave theory (Newell 1993) and the node model that utilizes route choice to depict flow propagation throughout the network. Network users may encounter a different experienced travel time than the expected travel time as a result of the DNL. If more than one destination are present, a multi-commodity DNL is utilized.

Two main causes could create a pedestrian traffic shockwave. First, a reduction in the link width leads to reduction in link capacity and as a result, a shockwave forms. In freeway traffic, a sudden capacity drop may lead to shockwave formation (Wu and Liu 2011). Similarly a shockwave can emerge in unidirectional pedestrian traffic as well (Helbing and Molnar 1995, Zhang et al. 2013). In this study, shockwave speed is constant and does not vary based on the free flow speed.

Secondly, pedestrian flow from one direction decreases the effective capacity of the other direction. This phenomenon isn't yet fully understood and has only been explored in a few past studies (Zhang 2015, Feliciani, Murakami, and Nishinari 2018, Fujita et al. 2019).

### 2.2.1. Link Model

Long, Gao, and Szeto (2011) proposed link travel time functions that are flow dependent as either a step function or a linear interpolation function. The function, however, does not capture the spillback effect. An alternative is using the fundamental relationship between flow and density. Flötteröd and Lämmel (2015) proposed a pedestrian bidirectional fundamental diagram that was calibrated with empirical data. The fundamental diagram proposed by Flötteröd and Lämmel (2015) provides a good representation of pedestrian bidirectional dynamics. However, it cannot be used in the original LTM framework (Yperman, Logghe, and Immers 2005, Yperman, Tampere, and Immers 2007) as the original LTM requires a triangular fundamental diagram (Newell 1993) to keep track of the traffic state. Several later studies extended the LTM formulations with piece-wise linear and concave FDs (Yperman, Tampere, and Immers 2007, Gentile et al. 2010, van der Gun, Pel, and van Arem 2017, Bliemer and Raadsen 2019, Raadsen and Bliemer 2019).

Here, we use a triangular FD and propose a three-dimensional extension to bidirectional pedestrian streams similar to what was previously proposed in Flötteröd and Lämmel (2015). The proposed triangular bidirectional FD can be constructed from free flow speed  $v_f$ , shock wave speed  $\omega$ , and jam density  $k_j$  as expressed in Equation (5) - (9). The density ratio  $\rho_a$  represents the ratio of the density of the reference direction over the density of the opposite direction in a bidirectional stream. The effective jam density  $\hat{k}_{jam,a}$  represents the practical jam density of the reference direction considering the density from the opposite direction. Similarly, the effective free flow speed  $\hat{v}_{f,a}$  represents the free flow speed considering the bidirectionality effects. Consider a pair of links  $a, a' \in A$  which belong to the same bidirectional stream. Let  $k_a$  and  $k_{a'}$  be density of link  $a$  and  $a'$ , respectively. Let  $\rho_a$  be the density ratio expressed as

$$\rho_a = \frac{k_a}{k_a + k_{a'}} \quad (5)$$

Let  $\hat{k}_{jam,a}$  be the effective jam density which is proportional to density ratio and can be defined as

$$\hat{k}_{j,a} = \rho_a k_{j,a} \quad (6)$$

Let  $k_{c,a}$  be the critical density defined as

$$k_{c,a} = \frac{\hat{k}_{j,a} \omega_a}{\hat{v}_{f,a} + \omega_a} \quad (7)$$

where  $\omega_a$  denotes the shockwave speed of link  $a$  and  $\hat{v}_{f,a}$  denotes the effective free flow speed of link  $a$  that can be defined in different ways as

$$\hat{v}_{f,a} = \frac{v_{f,a}}{e^{1-\rho_a}} \quad (8a)$$

$$\hat{v}_{f,a} = \rho_a^\gamma v_{f,a} \quad (8b)$$

where  $v_{f,a}$  denotes the free flow speed of link  $a$ ,  $\gamma$  denotes the model parameter for calibration. Equation (8a) expresses the relationship between density ratio and free flow speed as a logistic function while Equation (8b) expresses the relationship as a power function. The density ratio decreases if the number of pedestrians from the direction of interest decreases or the number of pedestrians from the opposite direction increases. As density ratio reduces, effective speed becomes slower which is reflected in Equation (8). However, for unidirectional flows, the effective speed would be identical with free flow speed and both Equation (8a) and Equation (8b) would be equivalent. The reduction in speed suggests that pedestrians experience a lower manoeuvrability and freedom to move as higher number of pedestrians flow from the opposite direction. In this study, we assume that the shockwave speed remains constant independent of the density ratio. Figure 2 provides a comparison between the FD proposed by Flötteröd and Lämmel (2015) and the proposed three dimensional triangular bidirectional FD in this study for use in the LTM. The three-dimensional triangular bidirectional FDs are calibrated using pedestrian trajectory data from a set of controlled bidirectional experiments (Zhang et al. 2012, Boltes and Seyfried 2013) with up to 350 participants. Pedestrian traffic density and flow measurements are then estimated using extended Edie's definitions to three-dimensional time-space diagrams (Saber and Mahmassani 2014).

An upstream link boundary can either be at free flow state or congested state, implying either hypocritical or hypercritical flow state in the fundamental diagram. Based on the traffic flow fundamental identity  $q = vk$ , we express flow and density relationship as follows

$$q_a(k_a) = \hat{v}_{f,a} k_a \quad \text{if } k_a \leq k_{c,a} \quad (9a)$$

$$q_a(k_a) = \omega_a(\hat{k}_{jam,a} - k_a) \quad \text{if } k_a > k_{c,a} \quad (9b)$$

The logistic function has its capacity closer to the capacity in Flötteröd and Lämmel (2015) FD, while the power function has a closer jam density. It is more important to have a closer capacity than jam density since a shockwave occurrence is less common than a capacitated flow. The jam density is utilized less frequently than sending flow is at its capacity. So, we decided to use the logistic function in the case studies.



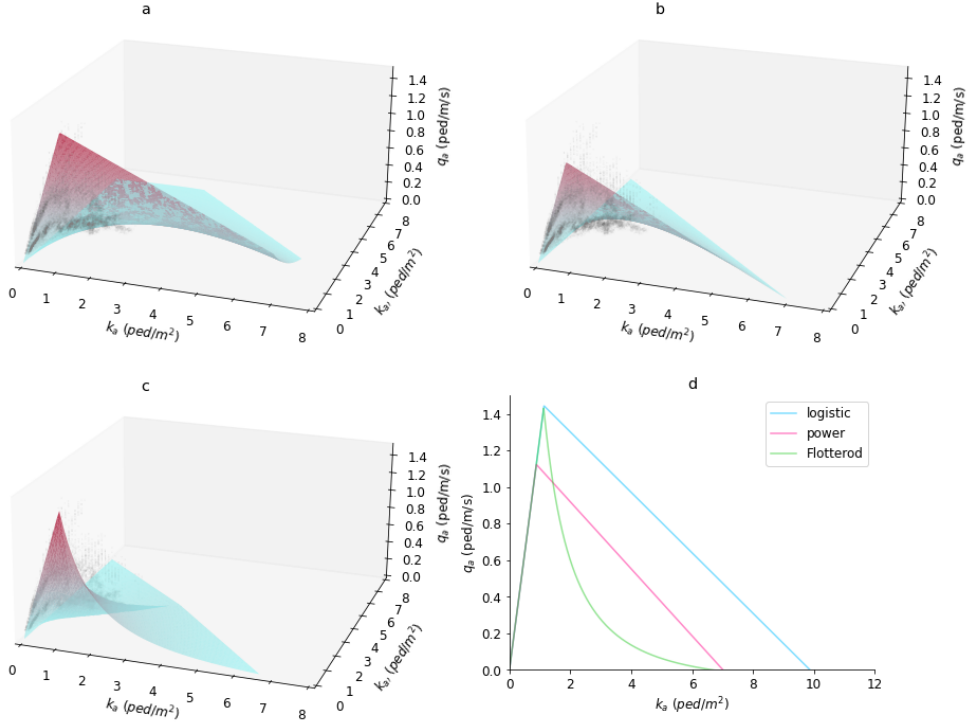


**Figure 2:** Three dimensional bidirectional fundamental diagram based on (a) a logistic function (b) a power function (c) the function proposed by Flötteröd and Lämmel (2015). Grey points represent empirical data used for calibration (d) A comparison between three FDs for unidirectional flow when density ratio  $\rho_a = 1$ .

Yperman, Logghe, and Immers (2005) proposed a numerical solution for the LTM that estimates the sending flow  $S_i$  of an incoming link  $i$  and the receiving flow  $R_j$  of an outgoing link  $j$ . Equation (10a) expresses the upstream boundary condition at time  $t$  as the outflow of incoming link  $i$  to a node between time  $t$  and  $t + \Delta t$ . Link capacity condition is defined as the maximum flow that can be sent from incoming link  $i$  limited to its capacity as expressed in Equation (10b). Sending flow  $S_i(t)$  is restricted by both conditions as expressed in Equation (10c).

$$S_{i,boundary}(t) = U_i(t + \Delta t - L_i/\hat{v}_{f,i}) - V_i(t) \quad (10a)$$

$$S_{i,link}(t) = C_i \Delta t \quad (10b)$$

$$S_i(t) = \min(S_{i,boundary}(t), S_{i,link}(t)) \quad (10c)$$

where  $U_i(t)$  denotes the cumulative number of pedestrians that pass through upstream of incoming link  $i$  at time  $t$ . Similarly the downstream boundary condition at time  $t$  is the inflow of outgoing link  $j$  from a node between time  $t$  and  $t + \Delta t$  as expressed in Equation (11a). Link capacity condition is defined as the maximum flow that can be sent from outgoing link  $j$  limited to its capacity as expressed in Equation (11b). Receiving flow  $R_j(t)$  is restricted by both conditions as expressed in Equation (11c).

$$R_{j,boundary}(t) = V_j(t + \Delta t - L_j/\hat{v}_{w,j}) + k_{j,j} L_j - U_j(t) \quad (11a)$$

$$R_{j,link}(t) = C_j \Delta t \quad (11b)$$

$$R_j(t) = \min(R_{j,boundary}(t), R_{j,link}(t)) \quad (11c)$$

where  $V_j(t)$  denotes the cumulative number of pedestrians that pass through downstream of outgoing link  $j$  at time  $t$ .

Both sending and receiving flows are constraints to limit how many flows can travel from/to any link. In the next

subsection, actual flows are regulated by a node model to maximize the total flow  $q_{ij}^n$  from incoming links  $i$  to outgoing links  $j$  through node  $n \in N$  while satisfying the constraints.

### 2.2.2. Node Model

Several studies in the literature have explored node merging and diverging behaviors (Daganzo 1995a, Bliemer 2007, Gentile et al. 2010, Smits et al. 2015). Here, we follow a generic class of first order macroscopic node model formulation (Tampère et al. 2011) that transfers total flows consistently over all nodes in the network (Himpe, Corthout, and Tampère 2016, Raadsen, Bliemer, and Bell 2016). Let  $N$  be a set of nodes in the network and  $q_{ij}^n$  be the flow from incoming link  $i$  toward outgoing link  $j$  through node  $n$ . Let  $S_i^n$  be the demand constraint as the maximum flow that incoming link  $i$  could possibly send if the node  $n$  and outgoing link(s) impose no restriction. Let  $R_j$  be the supply constraint as the maximum flow that outgoing link  $j$  could possibly receive if the node  $n$  and incoming link(s) impose no restriction. Let  $\phi_{ij}^n$  be the turning fraction of node  $n$  from the incoming link  $i$  toward the outgoing link  $j$  which is defined as the ratio of the total flow from the incoming link  $i$  to the outgoing link  $j$  over total incoming flows from link  $i$ .  $j'$  is the incoming link of the same bidirectional stream. The node model is then formulated as a maximization problem as follows:

$$\text{maximize} \quad \sum_i \sum_j q_{ij}^n \quad \forall n \in N \quad (12a)$$

$$\text{subject to:} \quad q_{ij}^n \geq 0, \quad \forall i, j \quad (12b)$$

$$q_i^n = \sum_j q_{ij}^n \leq S_i^n, \quad \forall i \quad (12c)$$

$$q_j^n + \tilde{S}_j^n = \sum_i q_{ij}^n + \left( U_{j'}(t + \Delta t - L_j/v_{f,i}) - U_{j'}(t - L_j/v_{f,i}) \right) \leq R_j^n, \quad \forall j, j' \quad (12d)$$

$$\phi_{ij}^n = \frac{S_{ij}^n}{S_i^n} = \frac{q_{ij}^n}{q_i^n}, \quad \forall i, j \quad (12e)$$

Equation (12b) imposes a restriction that traffic would never flow backward as a non-negativity constraint. Conservation of flow is ensured with Equation (12c) and (12d) as the demand and supply constraints, respectively. The supply constraint consists of two terms,  $\sum_i q_{ij}^n$  represents the sum of all incoming link flows going toward outgoing link  $j$ . While the other term represents inflow of incoming links  $j'$  which is on the same bidirectional stream as outgoing link  $j$ , taking into account the “look ahead” behavior of the opposite direction prior to reaching node  $n$ . Equation (12e) enforces conservation of turning fractions (CTF) which ensures the ratio of partial demand  $S_{ij}^n$  over the total demand  $S_i^n$  is equal to the ratio of partial flow  $q_{ij}^n$  over the total flow  $q_i^n$ . CTF condition is equivalent to the first-in-first-out (FIFO) condition (Tampère et al. 2011). If the flow is restricted by one of the outgoing links, the total flows will be the scaled-down version of the total demand. This condition prevents node model from unrealistically preferring any flows over others. Furthermore, the invariance principle condition is automatically satisfied since  $q_{ij}$  is derived by distributing supply and not the demand (Tampère et al. 2011).

Overall, the node model regulates how many pedestrians pass through node  $n$  at time  $k$  after pedestrians already decide which paths to take. However, pedestrians that are traveling in the network may adjust their path based on dynamically changing traffic conditions.

Here, we provide a simple example to demonstrate how the node model can be applied. A standard intersection consisting of four incoming and four outgoing links is considered as shown in Figure 3. From the given demand in Table 1, the total flows  $q_{ij}^n$  are restricted by several constraints as expressed in Equations (12b) - (12e).

In Table 1, the first column represents the demand toward link  $a'$  which is originated from only link  $b$  as  $S_{ba'}$ . From Equation (12c), the demand constraint limits the flow  $q_{ba'} \leq S_b$  which must be less than 1.5. From the supply constraint Equation (12d), we can rewrite the equation to determine the total flow as  $q_{ba'} \leq R_{a'} - \tilde{S}_{a'}$ . Since the supply constraint  $R_{a'}$  is equal to 3 and the demand on the same bidirectional link  $a'$  can be interpreted as  $\tilde{S}_{a'} = S_a = 1$ , the total flow  $q_{a'}$  will be no greater than 2. From the Equation (12e), we can rewrite the partial flow as  $q_{ba'} = \frac{S_{ij} q_i}{S_i} = \frac{S_{ba'} q_b}{S_b} = \frac{(1)(1.5)}{1.5} = 1$ . This shows that the partial flow  $q_{ba'}$  is limited by the demand constraint.

The second column represents the demand toward link  $b'$  which is originated from only link  $a$  as  $S_{ab'}$ . From



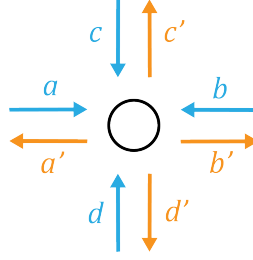


Figure 3: A node model example

Table 1: Demand  $S_{ij}$ 

$S_{ij}$	$a'$	$b'$	$c'$	$d'$	$S_i$
$a$	0	1	0	0	1
$b$	1	0	0	0.5	1.5
$c$	0	0	0	1	1
$d$	0	0	0	0	0
$\sum_i S_{ij}$	1	1	0	1.5	
$\tilde{S}_j$	1	1.5	1	0	
$R_j$	3	2	2	1	

Table 2: Flow  $q_{ij}$ 

$q_{ij}$	$a'$	$b'$	$c'$	$d'$	$q_i$
$a$	0	0.5	0	0	0.5
$b$	1	0	0	0.5	1.5
$c$	0	0	0	0.5	0.5
$d$	0	0	0	0	0
$\sum_i q_{ij}$	1	0.5	0	1	
$\sum_i q_{ij} + \tilde{S}_j$	2	2	1	1	

Equation (12c), the demand constraint limits the flow  $q_{ab'} \leq S_a$  which must be less than 1. From the supply constraint in Equation (12d), the total flow toward link  $b'$  can be expressed as  $q_{ab'} \leq R_{b'} - \tilde{S}_{b'}$ . Since the supply constraint  $R_{b'}$  is equal to 2 and the total demand on the same bidirectional flow can be expressed as  $\tilde{S}_{b'} = S_b = S_{ba'} + S_{bd'} = 1 + 0.5 = 1.5$ , the total flow  $q_{b'}$  is no greater than 0.5. From the Equation (12e), the partial flow can be expressed as  $q_{ab'} = \frac{S_{ij}q_i}{S_i} = \frac{S_{ab'}q_a}{S_a} = \frac{(1)(0.5)}{1} = 0.5$ . This shows that the partial flow  $q_{ab'}$  is limited by the supply constraint.

The fourth column represents demand toward link  $d'$  which are originated from link  $b$  and  $c$  as  $S_{bd'}$  and  $S_{cd'}$ , respectively. From Equation (12c), the demand constraint limits the total flow  $q_{d'} \leq S_{bd'} + S_{cd'}$  which must be less than 1.5. From the supply constraint in Equation (12d), the total flow toward link  $d'$  can be expressed as  $q_{d'} \leq R_{d'} - \tilde{S}_{d'}$ . Since the supply constraint  $R_{d'}$  is equal to 1 and the total demand on the same bidirectional flow can be expressed as  $\tilde{S}_{d'} = S_d = 0$ , the total flow  $q_{d'}$  is no greater than 1. From the Equation (12e), the partial flow can be expressed as  $q_{bd'} = \frac{S_{bd'}q_b}{S_b} = \frac{(0.5)(1.5)}{1.5} = 0.5$ . Similarly,  $q_{cd'} = \frac{S_{cd'}q_c}{S_c} = \frac{(1)(0.5)}{1} = 0.5$ . The partial flow  $q_{cd'}$  is limited by the supply constraint. However, the partial flow  $q_{bd'}$  is limited by both the demand and supply constraints.

Both the route choice model and DNL model must work together successively. The route choice model provides time-varying turning fractions specifically on each destination. Then the DNL utilizes turning fractions to simulate the propagation of pedestrians in the network under changing traffic states throughout the simulation. The first iteration of the route choice model performs on the empty network, so no pedestrian has been loaded into the network. The route choice model is based on a free flow route travel time directly proportional to distance. In this case, undertaken paths are simply the shortest paths. However, from the second iteration, the network has pedestrians still in the middle of their journey on the network. In this case, the route choice model adjusts to consider pedestrian traffic delays from

bidirectional traffic conditions following pVDFs.

### 3. Numerical Experiments

This section provides numerical experiments including two hypothetical networks and one real-world large-scale network to demonstrate the applicability and validity of the proposed pedestrian DTA modeling framework. Table 3 provides an overview summary of the settings for each of the numerical experiment scenarios.

To demonstrate that the obtained flow assignments are converging to DUE, we estimate the relative gap (Chiu et al. 2011) as expressed below

$$rel_{gap} = \frac{\sum_{k \in K} \sum_{r \in N} \sum_{s \in N} \sum_{p \in \Pi_{rs}} f_{p,k}^{rs} \hat{u}_{p,k}^{rs} - \sum_{k \in K} \sum_{r \in N} \sum_{s \in N} q_{rs}^k \hat{u}_{p,k}^{rs}}{\sum_{k \in K} \sum_{r \in N} \sum_{s \in N} q_{rs}^k \hat{u}_{p,k}^{rs}} \quad (13)$$

where  $\hat{u}_{p,k}^{rs}$  denotes the shortest route travel time of path  $p$  at departure time  $k$  between origin  $r$  and destination  $s$ .

#### 3.1. Small grid network

We first apply the proposed DTA framework on a small walking network consisting of 9 nodes and 24 links with 12 pairs of bidirectional links for demonstration purposes. Each link in the network is 4m wide and 2m long as shown in Figure 4a. We perform three hypothetical scenarios: Scenario 1 includes pedestrian travel demand for a single OD pair only, going from node 1 to node 9 as shown in Figure 4b. Scenario 2 includes pedestrian travel demand for two OD pairs, from node 1 to node 9 and from node 8 to node 4 as shown in Figure 4c. Scenario 3 includes the same travel demand as in scenario 1 as shown in Figure 4b; however after 20 seconds, a large travel cost is imposed on link 4-7 until the end of the simulation, creating a hypothetical link closure in the network. Figure 5 reveals the convergence pattern in scenarios 1, 2 and 3. The convergence of the bidirectional traffic in scenario 2 is slower than the unidirectional traffic in scenario 1 and 3.

We treat scenario 1 as the unidirectional baseline in which high pedestrian densities are likely to occur on links emanating from the origin node 1 and going to the destination node 9. All possible paths between the single OD pair inevitably include either link 1-4 or link 1-2 at the beginning and link 6-9 and link 8-9 at the end. All other links in the network will naturally end up having lower densities since flows will be distributed uniformly across the network in unidirectional streams. In scenario 1, flows are distributed evenly in the network as shown in Figure 6. Link densities on path 1-2-3-6-9 are also shown in Figure 9a. In scenario 2, the network is relatively more congested at the top part (e.g., node 4,5,7, and 8) as shown in Figure 7. Link densities on path 1-2-3-6-9 are higher than scenario 1 as shown in Figure 9b. The pedestrian route choice patterns in scenario 3 are similar to scenario 1 prior to  $t = 20$  seconds as shown in Figure 8 and 9c. Once the link closure at  $t = 20$  seconds is applied, link densities on path 1-2-3-6-9 increase. If a pedestrian begins a trip at  $t = 30$  seconds, the earliest trip completion time occurs in scenario 1, followed by scenario 3, and lastly scenario 2 as shown in Figure 9. The network in scenario 2 has the highest congestion level compared to the other two scenarios.

Overall, there are six possible paths connecting node 1 and node 9. As shown in Figure 10, between  $t = 8$  sec and  $t = 42$  sec, all path flows add up to 6 pedestrians/second. Paths colored in green include link 1-4 while paths colored in pink include link 1-2. For scenario 1 as shown in Figure 10a, flows on pink and green paths are roughly equal as expected since the grid network is totally symmetric and flows are unidirectional. For scenario 2, Figure 10b shows that the total flows on pink paths are dominant compared to the green paths suggesting that pedestrians prefer to go through link 1-2 rather than link 1-4. This reflects the impact of congestion from bidirectional pedestrian flows on link 4-7 and link 4-5 because of the presence of pedestrian flow from the opposite direction on link 7-4 and link 5-4. For

Table 3: Summary of the numerical experiment scenarios

Scenario	1	2	3*	4	5	6	Sydney
Nodes	9	9	9	10	10	10	3,341
Links	24	24	24	18	18	18	19,612
OD pairs	1	2	1	1	2	2	21,762

\* Significantly increase travel time of Link 7-8 after 20 seconds

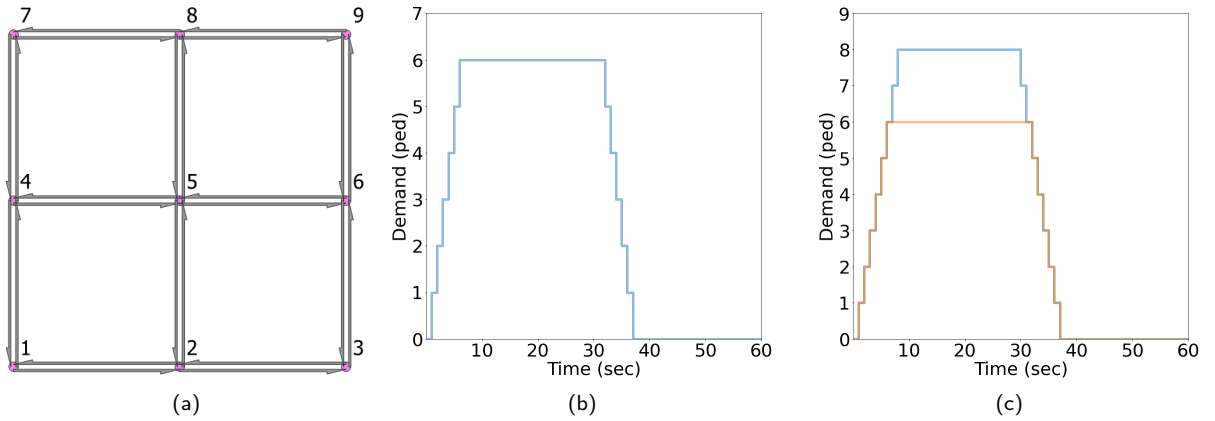


**Figure 4:** Small network demonstration: (a) the grid network structure. Pink circles represent nodes and gray lines with arrows represent directional links. (b) The demand profile for scenarios 1 and 3 with unidirectional flows. The black line represents demand from node 1 to node 9. (c) The demand profile for scenario 2 with bidirectional flows. The black line represents demand from node 1 to node 9 and the orange line represents demand from node 8 to node 4.

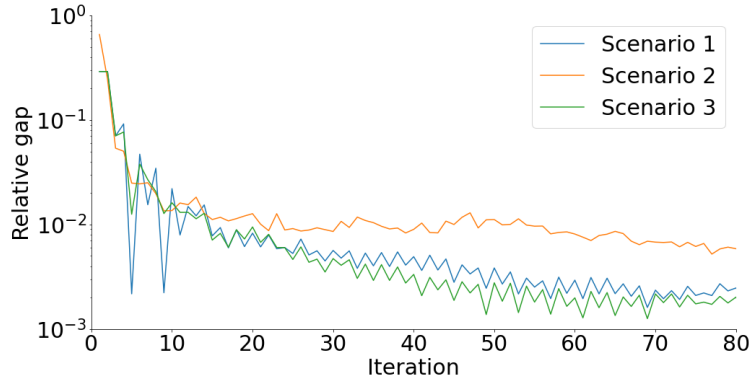


**Figure 5:** The convergence pattern in scenario 1, 2, and 3.

scenario 3, Figure 10c shows that after  $t = 20$  sec, no pedestrian takes path 1-4-7-8-9. This demonstrates the significant impact of introducing the link closure in the network and how pedestrians choose alternative routes when a part of the network is blocked.

As shown in Figure 11a, in scenario 1 with unidirectional flows only, both links 8-9 and 6-9 are utilized evenly. However, in scenario 2 when bidirectional flow is present, link 6-9 almost always experiences higher flow compared with link 8-9 suggesting that pedestrians tend to avoid the congested paths due to the presence of flow from the opposite direction. Figure 11b also shows that in scenario 3 after  $t = 20$  sec, no pedestrian uses link 7-8 due to the closure of link 4-7. While in scenario 1 without implementation of the link closure, link 7-8 was normally used by pedestrians.

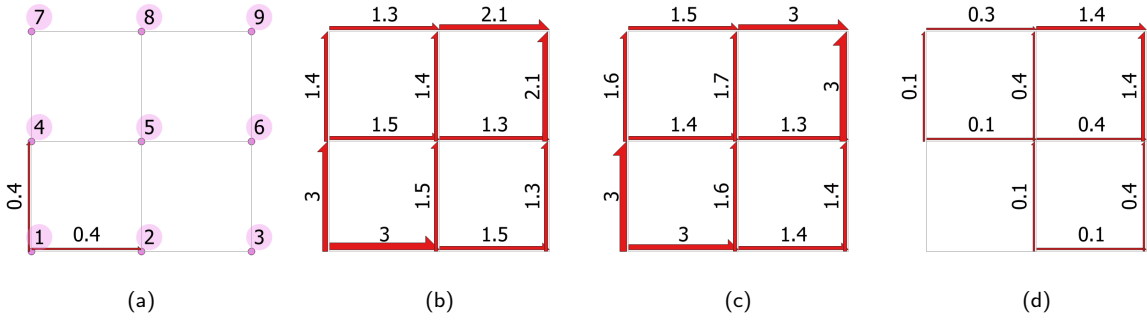


**Figure 6:** Simulation outcomes for scenario 1 over time: (a)  $t = 3$  sec (b)  $t = 10$  sec (c)  $t = 30$  sec (d)  $t = 40$  sec. The arrow thickness and the indicated numbers represent link outflows ranging 0-4 ped/sec.

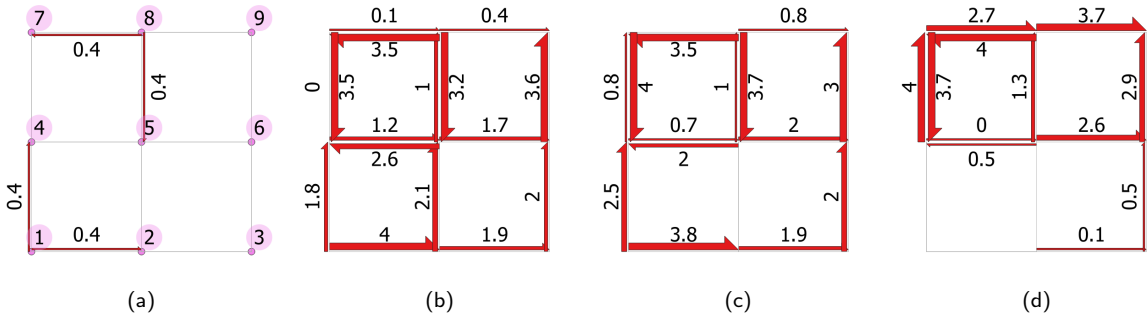


**Figure 7:** Simulation outcomes for scenario 2 over time: (a)  $t = 3$  sec (b)  $t = 10$  sec (c)  $t = 30$  sec (d)  $t = 40$  sec. The arrow thickness and the indicated numbers represent link outflows ranging 0-4 ped/sec.

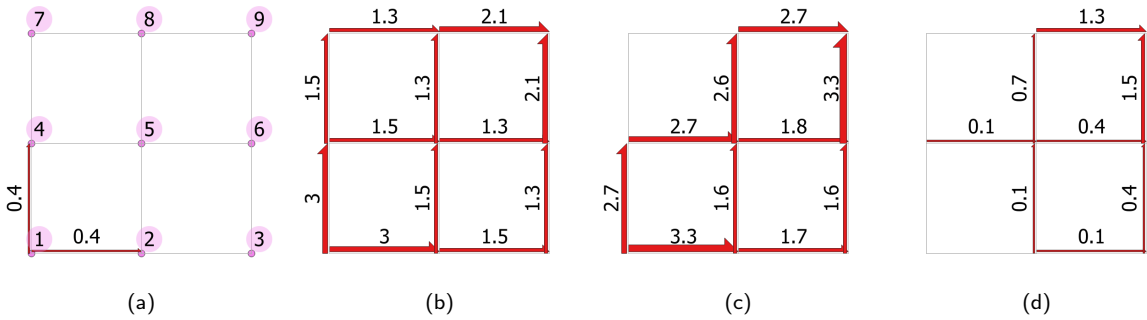


**Figure 8:** Simulation outcomes for scenario 3 over time: (a)  $t = 3$  sec (b)  $t = 10$  sec (c)  $t = 30$  sec (d)  $t = 40$  sec. The arrow thickness and the indicated numbers represent link outflows ranging 0-4 ped/sec.

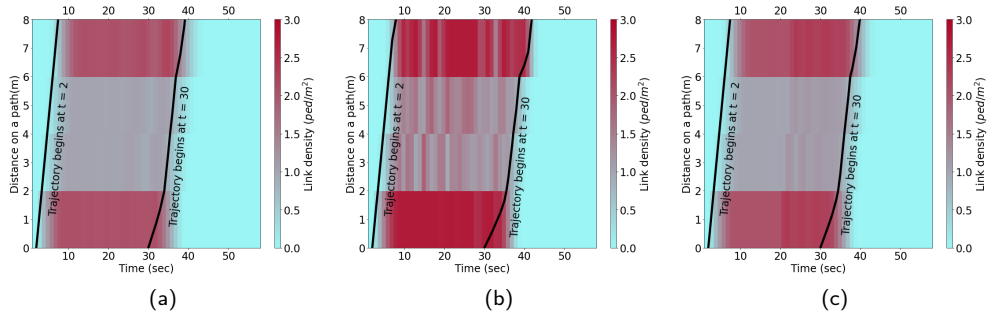


**Figure 9:** Simulation outcomes for path 1-2-3-6-9 for (a) scenario 1, (b) scenario 2 and (c) scenario 3. Time-space diagrams of link density are shown in  $\text{ped}/\text{m}^2$ . Grey lines represent example trajectories entering the network at  $t = 2$  and  $t = 30$  seconds.

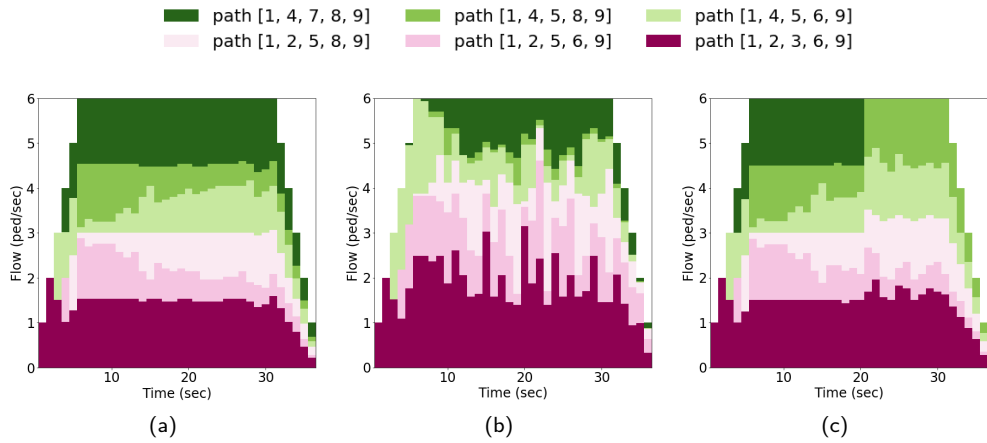


**Figure 10:** Distribution of path flows for (a) scenario 1, (b) scenario 2 and (c) scenario 3.

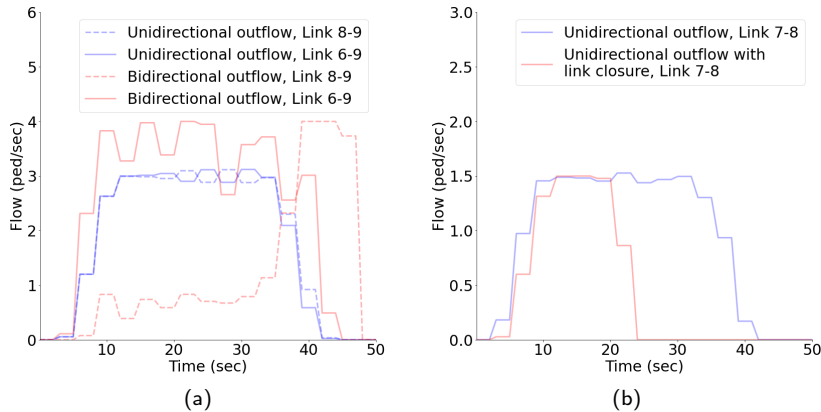


**Figure 11:** A comparative analysis of time-dependent link flows. Comparing scenario 1 with unidirectional flows shown in black against (a) scenario 2 with bidirectional flows shown in red for links 6-9 and 8-9 and (b) scenario 3 for link 7-8.

### 3.2. Long corridor

In this section, we apply the developed DPTA framework to a long bidirectional corridor to demonstrate the impact of directionality on pedestrian flows. The corridor consists of straight walking links that are 2m long and 4m wide.

We perform three hypothetical scenarios numbered continuously from the previous section: In scenario 4, we decrease the width of link 9-10 to create a bottleneck and to trigger formation of a shockwave. Pedestrian demand in scenario 4 gradually increases from  $t = 1$  sec to  $t = 4$  sec reaching 4 pedestrians/second. From  $t = 5$  sec to  $t = 80$  sec, demand remains constant at 4 pedestrians/second. From  $t = 80$  sec to  $t = 83$  sec, demand gradually drops to zero and remains zero until the end of the simulation as shown in Figure 12b.

Scenario 5 represents a bidirectional stream with unbalanced flows consisting of pedestrian demand going from node 1 to node 10 as the major stream and demand from node 10 to node 1 in the opposite direction as the minor stream. The demand for the major direction is identical to scenario 4. However, the demand for the minor direction gradually increases between  $t = 1$  sec and  $t = 4$  sec reaching 2 pedestrians/second. From  $t = 5$  sec to  $t = 50$  sec, demand remains constant at 2 pedestrian/second. From  $t = 50$  sec to  $t = 53$  sec demand gradually drops to zero and remains zero until the end of the simulation as shown in Figure 12c.

Scenario 6 represents a bidirectional stream with balanced flows at the beginning gradually turning into a unidirectional stream in which demand in both directions peak at 4 pedestrians/second. The demand for the minor direction begins to drop at  $t = 50$  sec while the demand for the major direction drops later at  $t = 80$  sec as shown in Figure 12d.

Since the corridor has only one path and one single OD pair, the model utilizes only one iteration of route choice. In scenario 4, pedestrians walk through the corridor with the maximum flow of 4 pedestrians/second from node 1 toward node 9. Once pedestrians reach the bottleneck on link 9-10, flow begins to drop as shown in Figure 13b. A shockwave forms on link 8-9 at distance 14-16 m and propagates backward with the speed of 0.18 m/s as shown in Figure 13a. However, after time  $t = 85$  second, as no demand loads into the network, a forward recovery shockwave forms on link 5-6 until the entire crowd exits the corridor.

In scenario 5, pedestrians move through the corridor with the maximum flow of 4 pedestrians/second for the major stream and 2 pedestrians/second for the minor stream as shown in Figure 14c and 14d. Once both pedestrian streams meet in the middle of the corridor at distance = 8 m, flows from both directions significantly drop. For the major direction, flow drops to 2 pedestrians/second from distance 10-18 m because the minor stream already occupies the available space to accommodate the flow of 2 pedestrians/second. The minor direction flow drops significantly at distance = 8 m as shown in Figure 14d. The walking speed in the minor direction also significantly reduces as pedestrians slowly make their way through as can be observed from the sharp reduction in the trajectories slope in the time-space diagram. Once the minor direction reaches node 1, it begins to block the major stream from entering the corridor as not all the flow can load into the network as shown in Figure 14c. When the two opposite streams meet, pedestrians take turn traversing through each node. Two shockwaves are also formed. As flow begins to drop in the major direction, a backward forming shockwave forms and propagates from distance 8 m as shown in Figure 14a. As the entire corridor is affected by the major direction, the minor direction stream exhibits a forward forming shockwave slowly penetrating through the major direction as shown in Figure 14b. In microscopic pedestrian models, gridlock is a common occurrence once the bidirectional traffic condition reaches the critical density, which causes pedestrians to halt all movements (Muramatsu, Irie, and Nagatani 1999, Nagatani 2009, Nowak and Schadschneider 2012, 2013, Tao and Dong 2017). However, there is no empirical evidence showing the existence of gridlock in the literature. In reality, pedestrian movements have high degrees of freedom leading to space adaptation to avoid gridlock occurrence. To overcome this technical limitation, Nowak and Schadschneider (2013) and Tao and Dong (2017) propose mechanisms to fix a gridlock. In our proposed node model, we propose a mechanism to avoid gridlock. Equation (12d) introduces a look ahead behavior that pedestrians who want to go through a node would check in the opposite direction to ensure that flows do not exceed the receiving flow. This mechanism causes stuttering behaviors in which pedestrians from each direction take a turn going through a node to avoid gridlock.

In scenario 6, four shockwaves are formed in both directions as shown in Figure 15a and 15b. A backward forming shockwave is formed at  $t = 30$  sec that propagates upstream due to significant increase in flow and density in the major direction. A forward forming shockwave is also formed at  $t = 30$  sec that propagates downstream as pedestrians from the opposite direction mix into the main direction flow. Two recovering shockwaves also occur in both directions after congestion begin to dissipate from  $t = 60$  sec. Flows in both directions significantly reduce once the two opposite streams meet at distance 8 m, then both directions take turn passing through nodes as shown in Figure 15c and 15d. The simulated bidirectional long corridor successfully exhibits the formation and propagation of shockwaves when link capacities change due to the bidirectional effects or inclusion of a bottleneck. Results suggest that the proposed



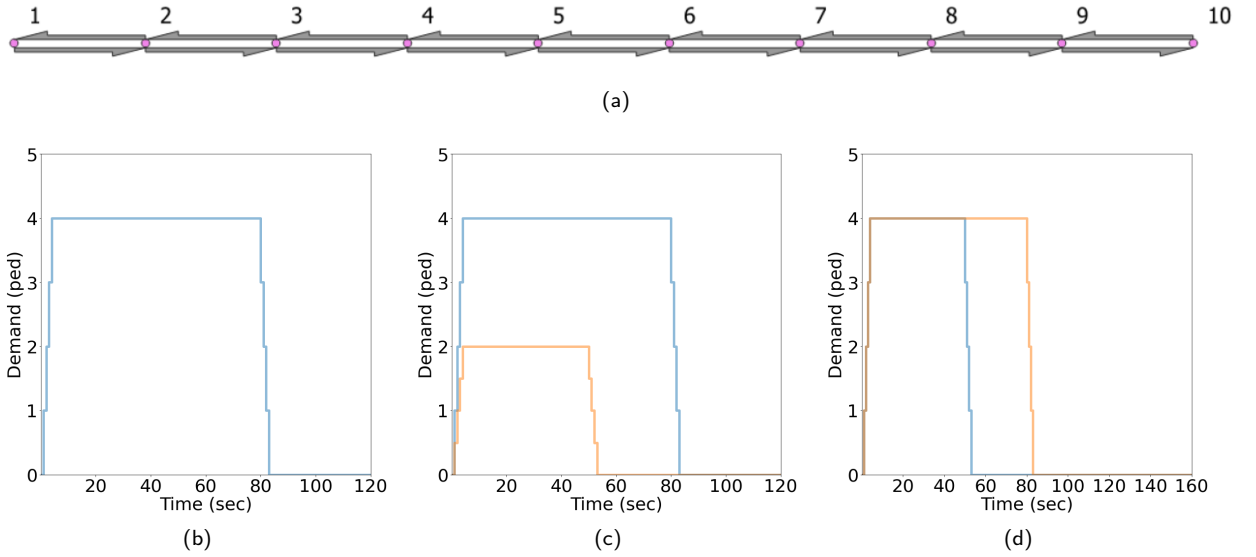


**Figure 12:** (a) Network structure of the modeled corridor. Pink circles represent nodes and grey lines with arrows represent directional links. Simulated demand profiles for the long corridor: (b) Scenario 4 with a bottleneck, (c) Scenario 5 with unbalanced bidirectional flows, and (d) Scenario 6 with balanced bidirectional flows. The black line represents demand from node 1 to node 10, referred to as major stream, and the orange line represents demand from node 10 to node 1, referred to as the minor stream.

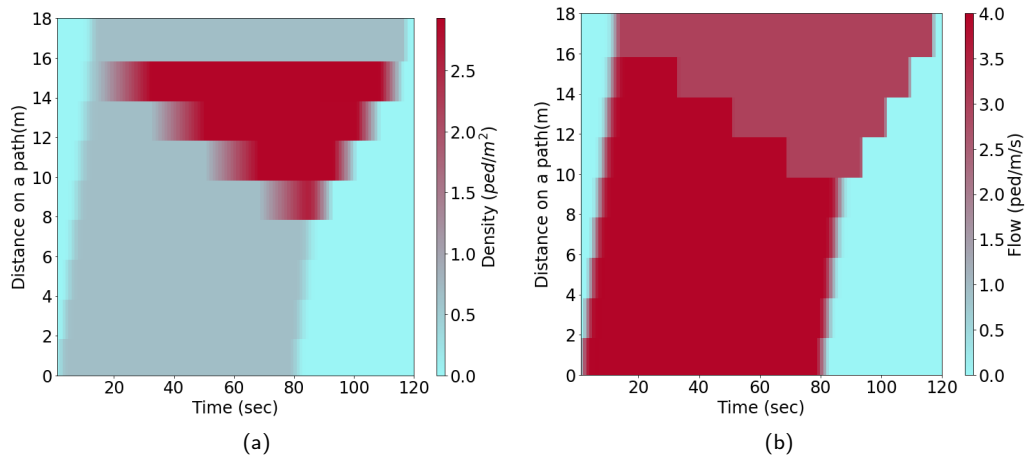


**Figure 13:** Time-space diagram of scenario 4 where pedestrians travel from node 1 toward node 10: (a) density in  $\text{ped}/\text{m}^2$  (b) flow in  $\text{ped}/\text{m}/\text{s}$ .

DPTA modeling framework reproduces reasonably realistic pedestrian dynamics compared to a static traffic assignment model.

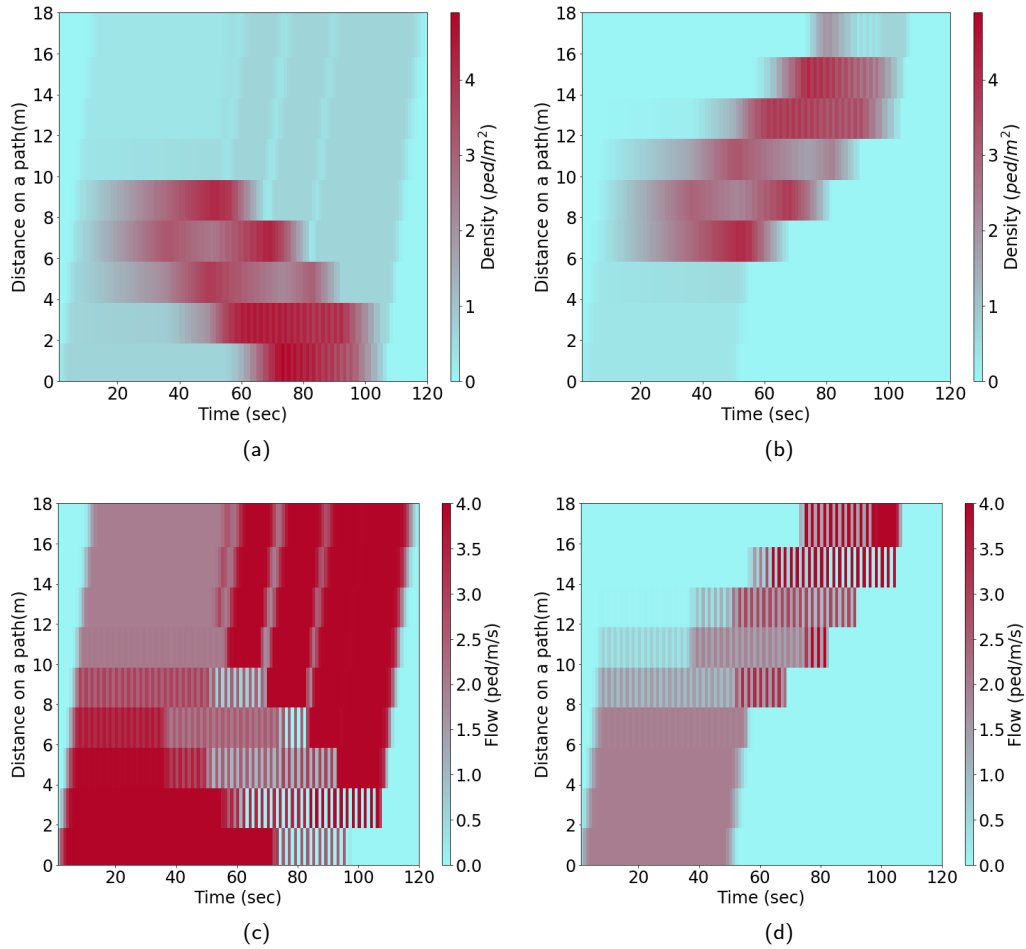


**Figure 14:** Time-space diagram of scenario 5. (a) density in  $\text{ped/m}^2$  of the major direction from node 1 toward node 10, (b) density in  $\text{ped/m}^2$  of the minor direction from node 10 toward node 1, (c) flow in  $\text{ped/m/s}$  of the major direction from node 1 toward node 10, and (d) flow in  $\text{ped/m/s}$  of the minor direction from node 10 toward node 1.

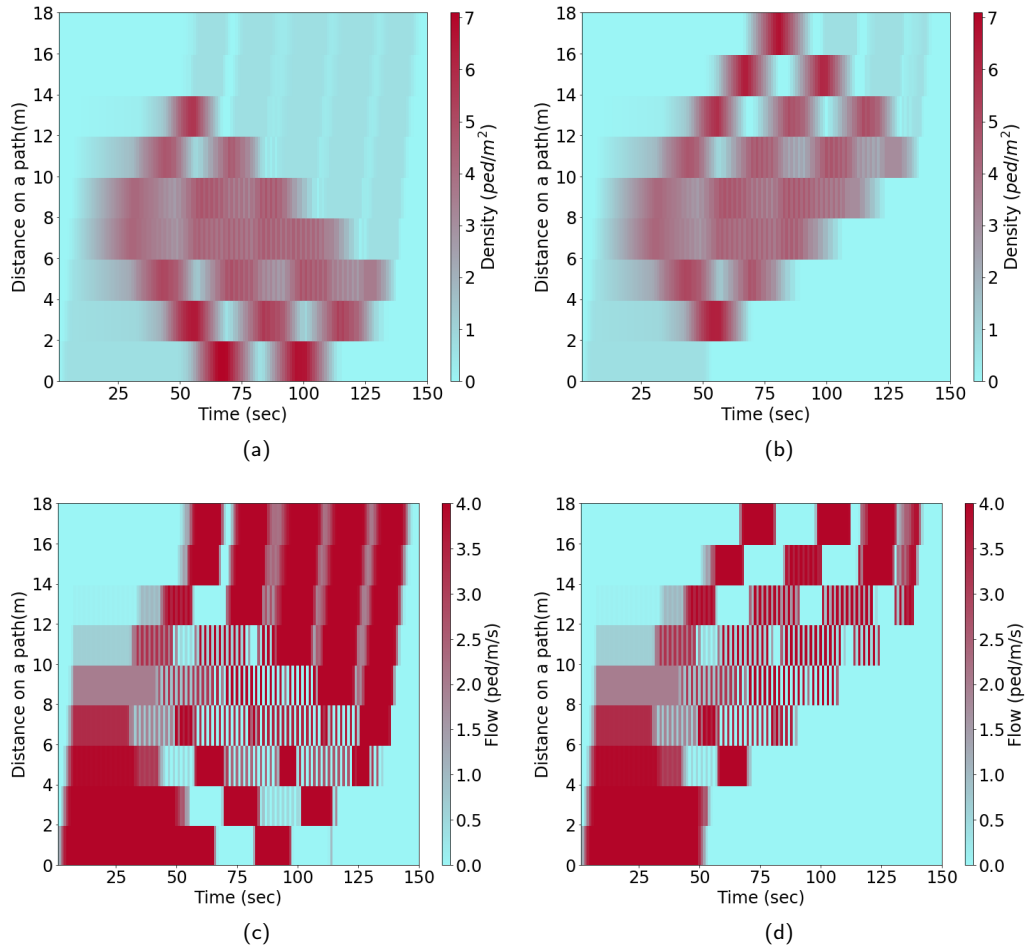


**Figure 15:** Time-space diagram of scenario 6. (a) density in  $\text{ped}/\text{m}^2$  of the major direction from node 1 toward node 10, (b) density in  $\text{ped}/\text{m}^2$  of the minor direction from node 10 toward node 1, (c) flow in  $\text{ped}/\text{m}/\text{s}$  of the major direction from node 1 toward node 10, and (d) flow in  $\text{ped}/\text{m}/\text{s}$  of the minor direction from node 10 toward node 1.

### 3.3. Large-scale real network application: Sydney footpath network

Here, we apply the proposed DPTA framework to model the sidewalk network in Sydney CBD as a large-scale example consisting of 2,327 nodes and 8,062 links. We have estimated a total travel demand of 28,414 walking trips during a 20-minute time window in the morning peak from 21,762 OD pairs based on information obtained from local transport authorities reports (Transport for NSW 2013) and commercially available data purchased from DSpark based on passively collected mobile phone traces. DSpark provides number of trips distinguished by travel mode between origin-destination pairs at the statistical area level 1 (SA1) aggregation. In this study, we only consider walking trips from/to the Sydney CBD area during an average weekday in October 2019 for a 20-minute interval in the morning peak. The origin-destination matrix is discretized from the SA1 level into smaller block level consistent with designed centroids in the network. Since the focus of this study is on formulation and development of a DPTA model using LTM, calibration of the OD walking demand remains a direction for future research. For this numerical experiment, we only conducted 3 iterations due to the size of the network and computational limitations.

Figure 16 shows the estimated link flows across the Sydney CBD network over time. At the beginning of the simulation, only a few links closer to public transportation stations, as the more significant origin nodes, are used as shown in Figure 16a and 16b. After 5 minutes, the footpath network becomes more congested as more links are being used as shown in Figure 16c and 16d.

The expected link travel time here is calculated from the pVDF as shown in Equation (3), while the experienced link travel time is calculated using the effective free flow speed from the FD as expressed previously in Equation (8). The expected route travel time in the route choice model is calculated instantaneously, while the experienced route travel time is calculated sequentially based on the entering time of each link. At the departure time, the expected or instantaneous travel time is considered as pre-trip information. However, post-trip information is necessary to determine the experienced travel time (Chiu et al. 2011). We formulated an instantaneous route travel time as shown in Equation (14a) and an experienced route travel time as shown in Equation (14b) similar to formulations proposed by Yildirimoglu and Geroliminis (2013).

$$c_{p,I}^{rs}(k) = \sum_{a \in A} \sum_{t \in T} c_{a,t} \delta_{a,p,k,t}^{rs} = \sum_{i=a}^I c_i^{pVDF}(k) \quad \forall p \in \Pi_{rs}, \forall k \in K \quad (14a)$$

$$c_{p,I}^{rs}(k) = \sum_{i=a}^I c_i^{FD}(k + c_{p,i}^{rs}(k)) \quad \forall p \in \Pi_{rs}, \forall k \in K \quad (14b)$$

where  $c_{p,I}^{rs}(k)$  denotes an accumulated travel time on path  $p$  connecting OD pair  $(r, s)$  exiting link  $I$  at departure time  $k$ ,  $A$  denotes a set of links,  $\Pi_{rs}$  denotes the set of paths connecting OD pair  $(r, s) \in W$ ,  $K$  denotes a set of departure time, path  $p$  consists of multiple links from  $a, \dots, I \in A$  ( $a$  is the most upstream link and  $I$  is the most downstream link),  $c_i^{pVDF}$  denotes the link travel time based on Equation (3), and  $c_i^{FD}$  denotes the link travel time derived from Equation (8).

The two are expected to have high correlation despite exhibiting slightly different patterns as shown in Figure 17. At the beginning of the simulation when the network is empty, experienced route travel times tend to be larger than the expected route travel times. However, 10 minutes into the simulation when the network becomes more congested, experienced route travel times tend to be even greater than the expected route travel times as shown in Figure 17(a). The distribution of experienced route travel times against expected route travel times are shown in Figure 17(b) for  $t = 0$  sec to  $t = 600$  sec and in Figure 17(c) for  $t = 600$  sec to  $t = 1200$  sec. The average experienced route travel time is greater than the expected route travel time. This results in a wider distribution of pedestrians across available paths in the network, preventing gridlocks to happen as a common limitation in many large-scale simulation-based DTA models (Mahmassani, Saberi, and Zockaie 2013). In Figure 17, we show two travel time distribution snapshots from  $t = 1$  sec and  $t = 601$  sec to demonstrate how the expected and experienced route travel times change at different traffic states. The difference between the expected and experienced travel time at  $t = 1$  sec the  $t = 601$  sec does not appear to be significant. We believe that the 28,414 trips used as travel demand might not be too high to produce heavily congested traffic states.

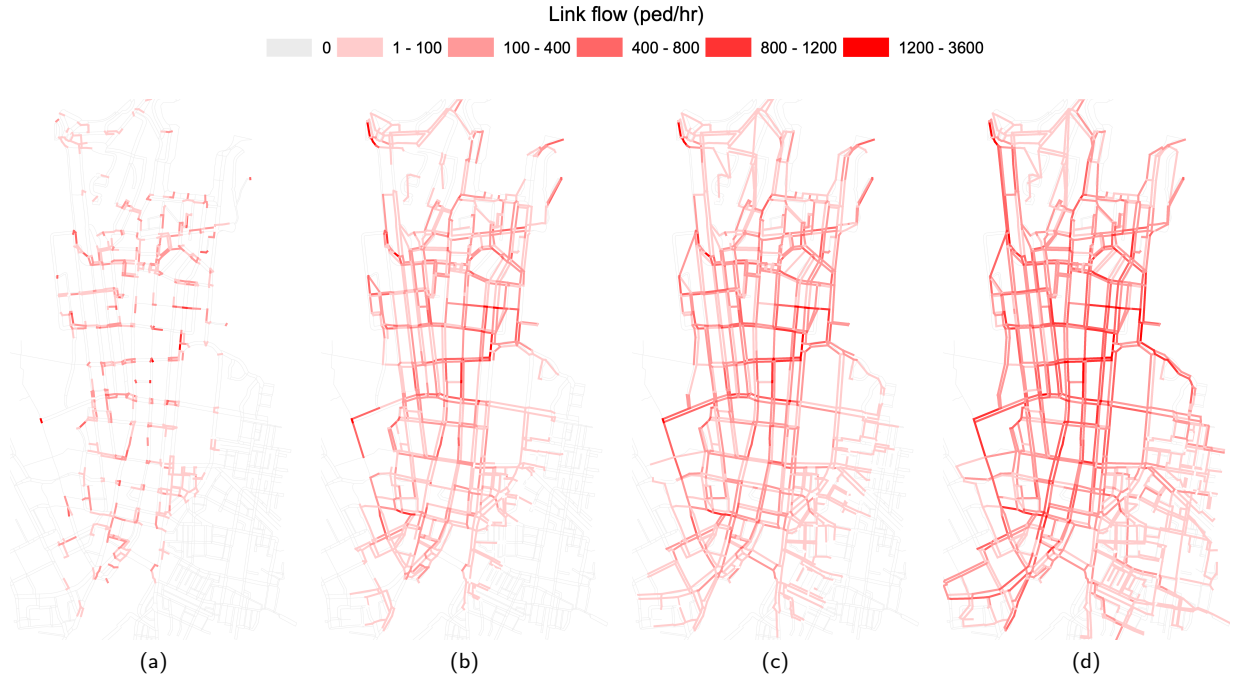


**Figure 16:** Simulation results of the Sydney footpath network at different times. Line thickness represents link outflows ranging from 0 - 3600 ped/hour. (a)  $t = 1$  min (b)  $t = 3$  min (c)  $t = 5$  min (d)  $t = 14$  min

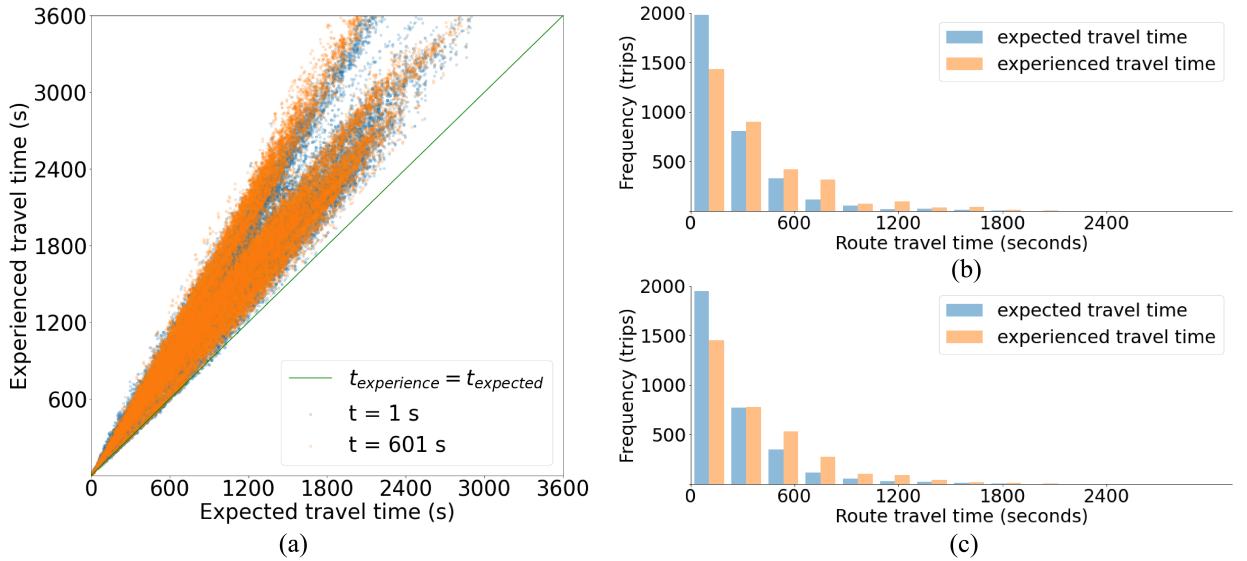


**Figure 17:** A comparison of the expected route travel times against experienced route travel times from the Sydney CBD footpath network: (a) Comparative scatter plot at  $t = 1$  sec and  $t = 601$  sec, (b) distribution of route travel times between  $t = 1$  and  $t = 300$  sec, and (c) distribution of route travel times between  $t = 601$  sec and  $t = 900$  sec.

## 4. Conclusion

In this paper, we proposed a DPTA framework specifically for pedestrian networks with bidirectional links. The study formulated and presented the DUE problem for walking networks accounting for the microscopic characteristics of bidirectional pedestrian streams often observed in crowded sidewalks and crossings such as dynamic lane-formation and self-organization. To reproduce realistic formation and dissipation of shockwaves in the network, we presented an adaptation of the LTM consisting of a link model and a node model. The link model regulates how pedestrians traverse on any link, including how congestion due to bidirectional traffic affects the speed of pedestrians and how a capacity drop creates shockwaves in both directions. The link model also captures the bidirectional impact using a three-dimensional triangular bidirectional FD. The node model regulates how pedestrians go through any nodes following non-negativity, conservation of bidirectional flows and turning fractions constraints.

We tested the developed DPTA modeling framework in a small grid network and a long corridor with strong bidirectional effects. Results from a small grid network successfully reproduced the pedestrians' behavior in avoiding routes with high travel time caused by the bidirectional effects and link closure. The simulated bidirectional long corridor successfully exhibited formation, propagation, and dissipation of shockwaves when link capacities change due to the bidirectional effects or introduction of a bottleneck. The paper also presented results from a large-scale sidewalk network model of Sydney CBD, demonstrating the applicability of the model to real-world networks.

Future research could further explore development of stochastic route choice models (Gentile 2016), adapting more efficient LTM algorithms (Raadsen and Bliemer 2019), developing network-wide pedestrian control strategies (Molyneaux, Scarinci, and Bierlaire 2021) in the proposed DPTA context, and develop a route choice model under system optimum condition to improve overall safety and efficiency for large pedestrian crowd events.

## Acknowledgement

This research was funded by the Australian Government through the Australian Research Council (project number DP220102382).

## References

- Aghamohammadi R, Laval JA, 2020 *Dynamic traffic assignment using the macroscopic fundamental diagram: A review of vehicular and pedestrian flow models. Transportation Research Part B: Methodological* 137:99–118.
- Batista SF, Leclercq L, 2019 *Regional dynamic traffic assignment framework for macroscopic fundamental diagram multi-regions models. Transportation Science* 53(6):1563–1590.
- Bliemer MC, 2007 *Dynamic queuing and spillback in analytical multiclass dynamic network loading model. Transportation research record* 2029(1):14–21.
- Bliemer MC, Bovy PH, 2003 *Quasi-variational inequality formulation of the multiclass dynamic traffic assignment problem. Transportation Research Part B: Methodological* 37(6):501–519.
- Bliemer MC, Raadsen MP, 2019 *Continuous-time general link transmission model with simplified fanning, part i: Theory and link model formulation. Transportation Research Part B: Methodological* 126:442–470.
- Bliemer MCJ, 2001 *Analytical Dynamic Traffic Assignment with Interacting User-Classes-Theoretical Advances and Applications using a Variational Inequality Approach*. Ph.D. thesis, Civil Engineering and Geosciences.
- Blue VJ, Adler JL, 2001 *Cellular automata microsimulation for modeling bi-directional pedestrian walkways. Transportation Research Part B: Methodological* 35(3):293–312.
- Boltes M, Seyfried A, 2013 *Collecting pedestrian trajectories. Neurocomputing* 100:127–133, URL <http://dx.doi.org/10.1016/j.neucom.2012.01.036>.
- Cao S, Seyfried A, Zhang J, Holl S, Song W, 2017 *Fundamental diagrams for multidirectional pedestrian flows. Journal of Statistical Mechanics: Theory and Experiment* 2017(3):033404.
- Chakraborty S, Rey D, Moylan E, Waller ST, 2018 *Link transmission model-based linear programming formulation for network design. Transportation Research Record* 0361198118774753.
- Chen H, Rakha HA, 2014 *Real-time travel time prediction using particle filtering with a non-explicit state-transition model. Transportation Research Part C: Emerging Technologies* 43:112–126.
- Chen HK, Hsueh CF, 1998 *A model and an algorithm for the dynamic user-optimal route choice problem. Transportation Research Part B: Methodological* 32(3):219–234.
- Chiu YC, Bottom J, Mahut M, Paz A, Balakrishna R, Waller S, Hicks J, 2011 *Dynamic traffic assignment: A primer (transportation research circular e-c153). Transportation Research E-Circular*.
- Colombo RM, Garavello M, Lécureux-Mercier M, 2011 *Non-local crowd dynamics. Comptes Rendus Mathématique* 349(13-14):769–772.
- Cristiani E, Piccoli B, Tosin A, 2011 *Multiscale modeling of granular flows with application to crowd dynamics. Multiscale Modeling & Simulation* 9(1):155–182.
- Dafermos S, 1980 *Traffic equilibrium and variational inequalities. Transportation science* 14(1):42–54.



- Daganzo CF, 1994 *The cell transmission model: A dynamic representation of highway traffic consistent with the hydrodynamic theory. Transportation Research Part B: Methodological* 28(4):269–287, URL [http://dx.doi.org/https://doi.org/10.1016/0191-2615\(94\)90002-7](http://dx.doi.org/https://doi.org/10.1016/0191-2615(94)90002-7).
- Daganzo CF, 1995a *The cell transmission model, part ii: network traffic. Transportation Research Part B: Methodological* 29(2):79–93.
- Daganzo CF, 1995b *Properties of link travel time functions under dynamic loads. Transportation Research Part B: Methodological* 29(2):95–98.
- Feliciani C, Murakami H, Nishinari K, 2018 *A universal function for capacity of bidirectional pedestrian streams: Filling the gaps in the literature. PloS one* 13(12):e0208496.
- Flötteröd G, Lämmel G, 2015 *Bidirectional pedestrian fundamental diagram. Transportation research part B: methodological* 71:194–212.
- Friesz TL, Bernstein D, Smith TE, Tobin RL, Wie BW, 1993 *A variational inequality formulation of the dynamic network user equilibrium problem. Operations research* 41(1):179–191.
- Friesz TL, Han K, Neto PA, Meimand A, Yao T, 2013 *Dynamic user equilibrium based on a hydrodynamic model. Transportation Research Part B: Methodological* 47:102–126.
- Friesz TL, Kim T, Kwon C, Rigdon MA, 2011 *Approximate network loading and dual-time-scale dynamic user equilibrium. Transportation Research Part B: Methodological* 45(1):176–207.
- Fujita A, Feliciani C, Yanagisawa D, Nishinari K, 2019 *Traffic flow in a crowd of pedestrians walking at different speeds. Physical Review E* 99(6):062307.
- Gentile G, 2016 *Solving a dynamic user equilibrium model based on splitting rates with gradient projection algorithms. Transportation Research Part B: Methodological* 92:120–147.
- Gentile G, et al., 2010 *The general link transmission model for dynamic network loading and a comparison with the due algorithm. New developments in transport planning: advances in Dynamic Traffic Assignment* 178:153.
- Haghani M, 2020a *Empirical methods in pedestrian, crowd and evacuation dynamics: Part i. experimental methods and emerging topics. Safety science* 129:104743.
- Haghani M, 2020b *Empirical methods in pedestrian, crowd and evacuation dynamics: Part ii. field methods and controversial topics. Safety science* 129:104760.
- Haghani M, Sarvi M, 2018 *Crowd behaviour and motion: Empirical methods. Transportation research part B: methodological* 107:253–294.
- Han K, Eve G, Friesz TL, 2019 *Computing dynamic user equilibria on large-scale networks with software implementation. Networks and Spatial Economics* 19(3):869–902.
- Han K, Piccoli B, Szeto W, 2016 *Continuous-time link-based kinematic wave model: formulation, solution existence, and well-posedness. Transportmetrica B: Transport Dynamics* 4(3):187–222.
- Hänseler FS, Bierlaire M, Farooq B, Mühlematter T, 2014 *A macroscopic loading model for time-varying pedestrian flows in public walking areas. Transportation Research Part B: Methodological* 69:60–80.
- Hänseler FS, Lam WH, Bierlaire M, Lederrey G, Nikolić M, 2017 *A dynamic network loading model for anisotropic and congested pedestrian flows. Transportation Research Part B: Methodological* 95:149–168.
- He X, Liu HX, 2012 *Modeling the day-to-day traffic evolution process after an unexpected network disruption. Transportation Research Part B: Methodological* 46(1):50–71.
- Helbing D, Molnar P, 1995 *Social force model for pedestrian dynamics. Physical review E* 51(5):4282.
- Himpe W, Corthout R, Tampère MC, 2016 *An efficient iterative link transmission model. Transportation Research Part B: Methodological* 92:170–190.
- Hoogendoorn SP, Daamen W, Knoop VL, Steenbakkers J, Sarvi M, 2018 *Macroscopic fundamental diagram for pedestrian networks: theory and applications. Transportation research part C: emerging technologies* 94:172–184.
- Hoogendoorn SP, van Wageningen-Kessels F, Daamen W, Duives DC, Sarvi M, 2015 *Continuum theory for pedestrian traffic flow: Local route choice modelling and its implications. Transportation Research Part C: Emerging Technologies* 59:183–197.
- Huang K, Zheng X, Cheng Y, Yang Y, 2017 *Behavior-based cellular automaton model for pedestrian dynamics. Applied Mathematics and Computation* 292:417–424.
- Hughes RL, 2002 *A continuum theory for the flow of pedestrians. Transportation Research Part B: Methodological* 36(6):507–535.
- Jang W, Ran B, Choi K, 2005 *A discrete time dynamic flow model and a formulation and solution method for dynamic route choice. Transportation Research Part B: Methodological* 39(7):593–620.
- Jin WL, 2015 *Continuous formulations and analytical properties of the link transmission model. Transportation Research Part B: Methodological* 74:88–103.
- Lighthill MJ, Whitham GB, 1955 *On kinematic waves ii. a theory of traffic flow on long crowded roads. Proceedings of the Royal Society of London. Series A. Mathematical and Physical Sciences* 229(1178):317–345.
- Lilasathapornkit T, Rey D, Liu W, Saberi M, 2020 *Traffic assignment problem for footpath networks with bidirectional links. arXiv:2012.03389*.
- Lo HK, Szeto WY, 2002 *A cell-based variational inequality formulation of the dynamic user optimal assignment problem. Transportation Research Part B: Methodological* 36(5):421–443.
- Long J, Gao Z, Szeto W, 2011 *Discretised link travel time models based on cumulative flows: formulations and properties. Transportation Research Part B: Methodological* 45(1):232–254.
- Løvås GG, 1994 *Modeling and simulation of pedestrian traffic flow. Transportation Research Part B: Methodological* 28(6):429–443.
- Mahmassani HS, Saberi M, Zockaie A, 2013 *Urban network gridlock: Theory, characteristics, and dynamics. Procedia-Social and Behavioral Sciences* 80:79–98.
- Melson CL, Levin MW, Hammit BE, Boyles SD, 2018 *Dynamic traffic assignment of cooperative adaptive cruise control. Transportation Research Part C: Emerging Technologies* 90:114–133.
- Molyneux N, Scarinci R, Bierlaire M, 2021 *Design and analysis of control strategies for pedestrian flows. Transportation* 48(4):1767–1807.
- Moussaïd M, Perozo N, Garnier S, Helbing D, Theraulaz G, 2010 *The walking behaviour of pedestrian social groups and its impact on crowd*

- dynamics. *PLoS one* 5(4):e10047.
- Moustaid E, Flötteröd G, 2021 *Macroscopic model of multidirectional pedestrian network flows*. *Transportation research part B: methodological* 145:1–23.
- Muramatsu M, Irie T, Nagatani T, 1999 *Jamming transition in pedestrian counter flow*. *Physica A: Statistical Mechanics and its Applications* 267(3-4):487–498.
- Nagatani T, 2009 *Freezing transition in bi-directional ca model for facing pedestrian traffic*. *Physics Letters A* 373(33):2917–2921.
- Newell GF, 1993 *A simplified theory of kinematic waves in highway traffic, part i: General theory*. *Transportation Research Part B: Methodological* 27(4):281–287.
- Nie YM, Zhang HM, 2010 *Solving the dynamic user optimal assignment problem considering queue spillback*. *Networks and Spatial Economics* 10(1):49–71.
- Nogal M, O'Connor A, Caulfield B, Martinez-Pastor B, 2016 *Resilience of traffic networks: From perturbation to recovery via a dynamic restricted equilibrium model*. *Reliability Engineering & System Safety* 156:84–96.
- Nowak S, Schadschneider A, 2012 *Quantitative analysis of pedestrian counterflow in a cellular automaton model*. *Physical review E* 85(6):066128.
- Nowak S, Schadschneider A, 2013 *A cellular automaton approach for lane formation in pedestrian counterflow*. *Traffic and Granular Flow'11*, 149–160 (Springer).
- Raadsen MP, Bliemer MC, 2019 *Continuous-time general link transmission model with simplified fanning, part ii: Event-based algorithm for networks*. *Transportation Research Part B: Methodological* 126:471–501.
- Raadsen MP, Bliemer MC, Bell MG, 2016 *An efficient and exact event-based algorithm for solving simplified first order dynamic network loading problems in continuous time*. *Transportation Research Part B: Methodological* 92:191–210.
- Ran B, Boyce DE, LeBlanc LJ, 1993 *A new class of instantaneous dynamic user-optimal traffic assignment models*. *Operations Research* 41(1):192–202.
- Ran B, Hall RW, Boyce DE, 1996 *A link-based variational inequality model for dynamic departure time/route choice*. *Transportation Research Part B: Methodological* 30(1):31–46.
- Richards PI, 1956 *Shock waves on the highway*. *Operations research* 4(1):42–51.
- Saberi M, Aghabayk K, Sobhani A, 2015 *Spatial fluctuations of pedestrian velocities in bidirectional streams: Exploring the effects of self-organization*. *Physica A: Statistical Mechanics and its Applications* 434:120–128, URL <http://dx.doi.org/10.1016/j.physa.2015.04.008>.
- Saberi M, Mahmassani HS, 2014 *Exploring areawide dynamics of pedestrian crowds: three-dimensional approach*. *Transportation research record* 2421(1):31–40.
- Saeedmanesh M, Geroliminis N, 2017 *Dynamic clustering and propagation of congestion in heterogeneously congested urban traffic networks*. *Transportation research procedia* 23:962–979.
- Schwandt H, Huth F, Bärwolff G, 2013 *A macroscopic model for intersecting pedestrian streams with tactical and strategical redirection*. *AIP Conference Proceedings*, volume 1558, 2209–2212 (American Institute of Physics).
- Seyfried A, Steffen B, Klingsch W, Boltes M, 2005 *The fundamental diagram of pedestrian movement revisited*. *Journal of Statistical Mechanics: Theory and Experiment* 2005(10):P10002–P10002, URL <http://dx.doi.org/10.1088/1742-5468/2005/10/p10002>.
- Shahhoseini Z, Sarvi M, Saberi M, 2018 *Pedestrian crowd dynamics in merging sections: Revisiting the “faster-is-slower” phenomenon*. *Physica A: Statistical Mechanics and its Applications* 491:101–111.
- Smits ES, Bliemer MC, Pel AJ, van Arem B, 2015 *A family of macroscopic node models*. *Transportation Research Part B: Methodological* 74:20–39.
- Taherifar N, Hamedmoghadam H, Sree S, Saberi M, 2019 *A macroscopic approach for calibration and validation of a modified social force model for bidirectional pedestrian streams*. *Transportmetrica A: Transport Science* 1–28.
- Tampère CM, Corthout R, Cattrysse D, Immers LH, 2011 *A generic class of first order node models for dynamic macroscopic simulation of traffic flows*. *Transportation Research Part B: Methodological* 45(1):289–309.
- Tao Y, Dong L, 2017 *A cellular automaton model for pedestrian counterflow with swapping*. *Physica A: Statistical Mechanics and its Applications* 475:155–168.
- Tong C, Wong S, 2000 *A predictive dynamic traffic assignment model in congested capacity-constrained road networks*. *Transportation Research Part B: Methodological* 34(8):625–644.
- Tordeux A, Lämmel G, Hänseler FS, Steffen B, 2018 *A mesoscopic model for large-scale simulation of pedestrian dynamics*. *Transportation research part C: emerging technologies* 93:128–147.
- Transport for NSW, 2013 *Sydney city centre access strategy*. NSW Government .
- van der Gun JP, Pel AJ, van Arem B, 2017 *Extending the link transmission model with non-triangular fundamental diagrams and capacity drops*. *Transportation Research Part B: Methodological* 98:154–178.
- Wardrop JG, 1952 *Road paper. some theoretical aspects of road traffic research*. *Proceedings of the institution of civil engineers* 1(3):325–362.
- Wu X, Liu HX, 2011 *A shockwave profile model for traffic flow on congested urban arterials*. *Transportation Research Part B: Methodological* 45(10):1768–1786.
- Xiong M, Lees M, Cai W, Zhou S, Low MYH, 2010 *Hybrid modelling of crowd simulation*. *Procedia Computer Science* 1(1):57–65.
- Yildirimoglu M, Geroliminis N, 2013 *Experienced travel time prediction for congested freeways*. *Transportation Research Part B: Methodological* 53:45–63.
- Yildirimoglu M, Sirmatel II, Geroliminis N, 2018 *Hierarchical control of heterogeneous large-scale urban road networks via path assignment and regional route guidance*. *Transportation Research Part B: Methodological* 118:106–123.
- Yperman I, Logghe S, Immers B, 2005 *The link transmission model: An efficient implementation of the kinematic wave theory in traffic networks*. *Proceedings of the 10th EWGT Meeting*, 122–127 (Poznan Poland).
- Yperman I, Tampère CM, Immers B, 2007 *A kinematic wave dynamic network loading model including intersection delays*. Technical report, Katholieke Universiteit Leuven.

- Zhang J, Klingsch W, Schadschneider A, Seyfried A, 2012 *Ordering in bidirectional pedestrian flows and its influence on the fundamental diagram. Journal of Statistical Mechanics: Theory and Experiment* 2012(02):P02002.
- Zhang Q, 2015 *Simulation model of bi-directional pedestrian considering potential effect ahead and behind. Physica A: Statistical Mechanics and its Applications* 419:335–348.
- Zhang X, Weng W, Yuan H, Chen J, 2013 *Empirical study of a unidirectional dense crowd during a real mass event. Physica A: Statistical Mechanics and its Applications* 392(12):2781–2791.
- Zhu F, Ukkusuri SV, 2015 *A linear programming formulation for autonomous intersection control within a dynamic traffic assignment and connected vehicle environment. Transportation Research Part C: Emerging Technologies* 55:363–378.